ELSEVIER

Catalysis Today 50 (1999) 413–427

CATALYSIS TODAY

Effects of highly dispersed ceria addition on reducibility, activity and hydrocarbon chain growth of a Co/SiO_2 Fischer–Tropsch catalyst

B. Ernst, L. Hilaire, A. Kiennemann*

Laboratoire d'Etude de la Réactivité Catalytique, des Surfaces et Interfaces (LERCSI), UMR CNRS 7515, Ecole de Chimie, Polymères et Matériaux (ECPM), 1 rue Blaise Pascal, 67008, Strasbourg, Cedex, France

Abstract

A series of $Co–CeO_2/SiO_2$ catalysts at cobalt iso-content (25 wt%) with various concentrations in cerium (4.5, 8.9, 21.5 and 38.2 wt%) and a 25 wt% Co/SiO_2 system have been characterized and tested in Fischer–Tropsch synthesis for the production of high molecular weight hydrocarbons (waxes). The effects of cerium oxide addition on the cobalt particle size, on the reducibility of the cobalt and on the catalytic performance (activity and selectivity) of a Co/SiO_2 catalyst have been studied. The catalysts have been prepared with an original method combining the coprecipitation of the precursors of cobalt and cerium by oxalic acid with the hydrolysis and condensation of the tetraethoxysilane. The crystallite size measurements (TEM) of Co_3O_4 and CeO_2, which are the only structures detected by XRD and XPS in oxidized samples, indicated that the presence of cerium had a dispersing effect on the cobalt. It was also found that the ceria was well dispersed on the silica support. The reduction experiments (TPR and XPS) under hydrogen at 673 K showed that the reduction rate of ceria supported on SiO_2 was similar to that of ceria with high specific surface area. The cobalt reduction degree decreased with the addition of cerium, even in low concentration. It was however equivalent for the Co/CeO_2, Co–Ce(38.2 wt%)/SiO_2 and Co/SiO_2 catalysts allowing to conclude that the extent of cobalt reduction at 773 K was not very much affected by the reduction state of ceria. The catalytic activities (TOF) (P=2 MPa, T=493 K, H_2/CO=2/1) of $Co–CeO_2/SiO_2$ and Co/SiO_2 catalysts were similar. With the addition of cerium significant changes in hydrocarbon selectivities were observed: decrease in C_{2+} hydrocarbon selectivity and production of gasoline to the detriment of the C_{22+} fraction (chain growth probability (α) from 0.82 to 0.87 for $Co–CeO_2/SiO_2$ catalysts and 0.92 for the unpromoted catalyst). This modification was attributed to a smaller cobalt particle size, to the specific adsorption/desorption properties of H_2 and CO on $Co–CeO_2/SiO_2$ catalysts and also to the possible presence of formate species, which could be formed on the partially reduced ceria pointed out by H_2 and CO TPD studies. The hydrogenation of these species could explain the additional methane production in the Fischer–Tropsch synthesis under pressure.

Keywords: Cobalt; Fischer–Tropsch synthesis; Carbon monoxide hydrogenation; Cerium oxide; Reducibility

1. Introduction

Cobalt-based catalysts are currently the best systems for obtaining paraffins of high molecular weight with little CO_2 or alcohol formation. In the past 15 years or so, many formulations, all including cobalt, have been patented [1–7]. Beside cobalt such catalysts are generally composed of a second metal (Re, Rh, Ru, Pt, etc.) and/or another oxide (ZrO_2, TiO_2, ThO_2, etc.) and various supports have been tried: SiO_2, Al_2O_3, ZSM-5, etc. The addition of a small amount of a

*Corresponding author. Fax: +33-3-88-41-68-63; e-mail: kiennemann@chimie.u-strasbg.fr

0920-5861/99/$ – see front matter
PII: S0920-5861(98)00519-7

second metal is believed to help the reduction of cobalt via a spill-over process of hydrogen adsorbed on the second metal (Ru [8,9], Rh [10], Pt [11]) onto cobalt oxide. The presence of a second metal allows also to improve the regeneration of deactivated systems [12]. The support, generally an oxide, can play a part in the activity and selectivity of these catalysts in many ways: it may favour the dispersion of metallic particles (SiO_2) [13], interact with the metal (TiO_2, ZrO_2) [14], exhibit interesting redox properties (CeO_2) [15] and/or modify the acidity of the system [16], or the possibility of recovering or migrating onto the metal (La_2O_3) [17].

Rare earth oxides have been largely used as promoters for the hydrogenation of CO on various metals: Ni [18–21], Fe [22], Rh [23], Ru [21,24] and Pd [25,26]. Several studies were performed at atmospheric pressure on cobalt–rare earth oxide catalysts [27], in particular on carbon supports, which are not widely used in Fischer–Tropsch synthesis [17,28,29]. The conclusions were better activities and higher selectivities towards alkenes. A study on a 10% Co–La/Al_2O_3 [17] catalyst showed that the addition of lanthanum had no effect on the activity but that the selectivity in C_{2+} and the alkenes/alkanes ratio increased with increasing lanthana content. More complex formulations such as $Co_aA_bLa_cCeO_x$ (A=alkaline earth, a=0–25%, b=5%, c=15%) [30] or more simple systems like Co/CeO_2 unsupported or supported on a $MgAl_2O_4$ spinel [31], or promoted with Ru [32,33] were tested under experimental conditions which were expected to favour chain growth (P=5–30 bar). They also exhibited high conversions of CO, important selectivites in C_{5+} together with high olefins/paraffins ratios. These changes were attributed to the basicity of promoted catalysts [17].

The role of ceria seems worth studying because there has been some controversy about it: partial reduction of CeO_2 can be expected to create new sites for the adsorption of CO, favouring the C–O bond rupture and increasing the activity [18]. However, it has also been argued that the reduction of ceria may lead to a covering of the active surface by the promoter, leading therefore to a decrease in the chemisorption capacity. In the latter case, the distribution of the hydrocarbons may be changed and the catalytic activity will be lower.

In this paper, we describe the characterization and the catalytic properties of 25% Co–CeO_2/SiO_2 systems with various contents of ceria (from 5.1 to 40.1 wt% cerium) as compared to a 25% Co/SiO_2 catalyst. The role of CeO_2 on the hydrocarbon distribution and the higher production of methane will be explained by the formation of formate species on ceria.

2. Experimental

2.1. Catalyst preparation

The choice of the preparation technique obeyed several motivations: the necessity of mastering the cobalt content with a good dispersion of the metallic phase and a homogeneous size distribution of the particles, high surface specific area and a limited cobalt–silica interaction to avoid the formation of unreducible species (cobalt silicate). The technique developed for Co/SiO_2 [34] was adapted to Co–CeO_2/SiO_2 and Co–CeO_2 catalysts [35]. Cobalt nitrate ($Co(NO_3)_2{\cdot}6H_2O$), cerium nitrate ($Ce(NO_3)_3{\cdot}6H_2O$), tetraethoxysilane (TEOS) ($Si(OC_2H_5)_4$) and oxalic acid ($H_2C_2O_4{\cdot}2H_2O$) were dissolved separately in ethanol at 343 K. The first three solutions were mixed together and then the oxalic acid solution was added (10 wt% excess) under strong stirring. The formation of cobalt oxalate results in the production of nitric acid which contributes to the acidity of the medium. This mixture was slowly dried by evaporation during which the TEOS was hydrolyzed by the hydrating water of the nitrates and the oxalic acid into $Si(OH)_4$ and condensed to form siloxane bonds. We have shown [34] the influence of the evaporation time on the surface specific area of the Co/SiO_2 calcined catalyst. The best choice was 6 h. The sample was then dried at 373 K for 12 h and calcined at 823 K for 5 h.

2.2. Experimental techniques

2.2.1. Characterization of the catalysts

X-ray diffraction (XRD) measurements were performed on the catalysts using the Cu K_α radiation of a Siemens D5000 powder diffractometer device. The XRD patterns were recorded for 2θ 20° and 80° with a 0.005° 2θ spacing and three seconds exposure time. The identification of the phases was made with the

help of the JCPDS files (joint committee on powder diffraction standards).

X-ray photoelectron spectra were measured in a Vacuum Generators ESCA3 apparatus using Al K_α radiation. The sample, pelleted (~0.05 g) and set on a sample-holder with a heating device (293 K<T<873 K), was treated with hydrogen at different reduction temperatures at atmospheric pressure in a preparation chamber. The binding energies were measured by taking the C1s peak of the contamination carbon at 284.8 eV as reference.

The apparatus used for the transmission electron micrographs was a Topcon EM-002B with an acceleration voltage of 200 keV and a resolution of 1.8 Å. The analysis of the chemical elements was done by EDS with a KEVEC analyser (diameter of the selected area: 14 nm).

2.2.2. Temperature programmed reduction (TPR)

The temperature programmed reduction (TPR) experiments were done by passing 6% H_2 in He at a total flow rate of 50 ml min^{-1} (temperature increase rate: 15 K min^{-1}) from 323 to 1173 K over the calcined catalyst (0.20 g). A TCD device monitors water formation. The measurements of the hydrogen consumption were realized on a χsorb (chemisorb) device with a gas flow rate of 20 ml min^{-1} of 5% H_2 in N_2 from 298 to 773 K (1 K min^{-1}).

2.2.3. Chemisorption and temperature programmed desorption (TPD)

Carbon monoxide adsorption was performed at room temperature and at atmospheric pressure. Diluted carbon monoxide (2.5% CO in He) was sent by pulse on the catalyst (0.05 g) previously reduced at 673 K. The non-adsorbed monoxide was determined by GC.

After reduction of the catalyst (0.2–1.0 g) in a diluted hydrogen flow (5% H_2 in Ar) up to 773 K, the temperature was increased to 493 K under hydrogen atmosphere. The amount of chemisorbed hydrogen was recorded during the temperature decrease from 493 to 298 K. A temperature programmed desorption was subsequently performed between 298 and 493 K under argon after flushing the apparatus of all the residual gas phase hydrogen. The amount of chemisorbed and temperature programmed desorbed hydrogen was followed by TCD.

2.2.4. Temperature programmed surface reaction (TPSR)

CO adsorption before the TPSR was performed under a flow of pure CO (15 ml min^{-1}) at room temperature with 0.2 g of catalyst. After flushing by helium, the temperature was increased under hydrogen flow (20 ml min^{-1}) from 298 to 773 K with a 5 K min^{-1} slope. CO, CO_2 and CH_4 were detected by GC.

The treatment of passivation was performed after reduction of the catalyst, under a flow of diluted oxygen (2.5% O_2 in He). After flushing by helium the process described previously was applied.

2.2.5. Catalytic tests

Prior to reaction, the catalysts (1.0 g) were reduced ex situ (P=0.1 MPa) at 673 K, in a tubular glass reactor (total reduction gas flow 5% H_2/N_2: 30 ml min^{-1}). The catalytic tests have been performed in a three-phase (slurry) reactor. The catalyst was suspended by stirring in olefin free *n*-octadecane (25 g) which is inert to synthesis gas. The operating conditions were the following: T=493 K, P=2 MPa, H_2/CO ratio=2, GHSV=2000 h^{-1}. The analysis of the gas phase was realized by GC with an on-line TCD (CO, CO_2 and CH_4, Carbosieve SII column, length: 3 m, diameter: 1/8 in.) and FID (C_1–C_6 hydrocarbons, Hayesep R column, length: 2.5 m, diameter: 1/8 in.). The organic liquid phase was analysed in two capillary columns: Chrompack (l=12 m, ϕ=0.25 mm, polymethylsiloxane 0.25 μm depth) for the hydrocarbon C_6–C_{20} hydrocarbon fraction and SGE (l=50 m, ϕ=0.53 mm, siloxane and carborane copolymer 0.15 μm depth) for the C_{20}–C_{60} hydrocarbon fraction.

The mean duration of a catalytic test varies from 48 to 56 h. Thus, the value of carbon monoxide conversion at that moment will be taken as initial activity.

The catalytic activity was expressed as the total carbon monoxide conversion, the conversion to hydrocarbons and the carbon dioxide. The specific activity noted TOF (h^{-1}) was defined as the number of converted CO moles by cobalt metal site and unit time. It was deduced from the number of converted CO moles by gram of cobalt and unit time multiplied by the molar mass of the cobalt divided by the degree of reduction and the dispersion of cobalt. The relation between particle size (d expressed in nm) and dispersion (%D) was given by the following equation:

$\%D = 6.59 \times S/d$, where S is the atomic density of cobalt by nm^2: 14.6 atom nm^{-2} for fcc cobalt crystallites.

The selectivity was expressed in gram atom of carbon for methane, C_{5+} hydrocarbons and alcohols (ROH) and in weight percentage for C_1 and the various hydrocarbon fractions: C_2–C_4, C_5–C_9, C_{10}–C_{13}, C_{14}–C_{21} and C_{22+} (waxes).

3. Results and discussion

3.1. Characterization of $Co–CeO_2/SiO_2$ and Co/CeO_2 catalysts

A preliminary study by XRD of the dried preparations of $Co–CeO_2/SiO_2$ has shown the presence of cobalt oxalate ($CoC_2O_4 \cdot 2H_2O$) and of a mixed cobalt–cerium oxalate ($CoCe(C_4H_7O_{12}) \cdot H_2O$), evidencing the coprecipitation of cobalt and cerium, which can favour a subsequent cobalt–cerium interaction.

We give in Table 1 the bulk composition (elemental analysis), the BET surface area and the cobalt oxide crystallite size (derived from XRD) for the $Co–CeO_2$ and $Co–CeO_2/SiO_2$ catalysts and also for Co/SiO_2 for comparison.

After calcination, the catalysts with higher cerium contents (Co/CeO_2, $Co–CeO_2(A)/SiO_2$ and $Co–CeO_2(B)/SiO_2$) exhibit clearly two crystalline structures: Co_3O_4 spinel and CeO_2 fluorite, as shown by XRD (Fig. 1). When the percentage of cerium is lower than 10% (samples $Co–CeO_2(C)/SiO_2$ and $Co–CeO_2(D)/SiO_2$), Co_3O_4 only is detected. From the broadening of the diffraction lines (Debye–Scherrer method), the crystallite size of ceria can be estimated, which shows that even for high cerium contents (samples $Co–CeO_2(A)/SiO_2$ 40.1% and $Co–CeO_2(B)/SiO_2$ 22.5%), the particles of ceria are well dispersed with 8.0 and 8.5 nm sizes, respectively. Identical sizes of CeO_2 (8 nm) were obtained with CeO_2/SiO_2 prepared by capillary impregnation [36]. We think that such a good dispersion is directly related with the preparation technique. Indeed, coprecipitation of a mixture of ammonium ceric nitrate and cobalt nitrate by ammonium carbonate led to aggregates composed of 5 nm ceria crystallites, as observed by TEM [33]. It seems that the formation of a mixed cobalt–cerium oxalate favours a good dispersion of ceria.

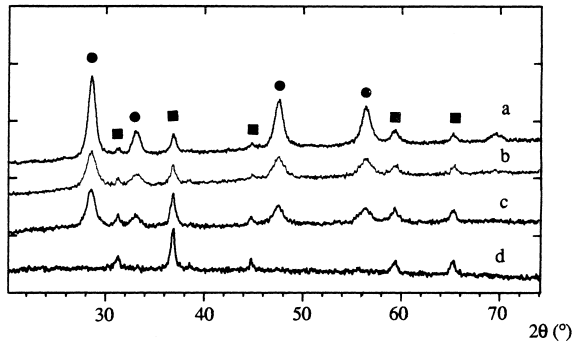

Fig. 1. XRD patterns for the $Co–CeO_2$ (a), $Co–CeO_2(A)/SiO_2$ (b), $Co–CeO_2(B)/SiO_2$ (c), $Co–CeO_2(C)/SiO_2$ (d) catalysts calcined at 823 K (references: Co_3O_4 (■), CeO_2 (●)).

Table 1
Catalyst composition, BET surface area and Co_3O_4 particle size of Co/SiO_2, $Co–CeO_2$ and $Co–CeO_2/SiO_2$ catalysts

Catalyst[a]	Composition (wt%)[b]				BET surface area ($m^2\ g^{-1}$)	Co_3O_4 particle size (nm)[c]
	Co	Si	Ce	O		
$Co–CeO_2$	25.7	–	52.8	21.3	65	20.5
$Co–CeO_2(A)/SiO_2$	25.5	7.4	40.1	26.0	137	18.5
$Co–CeO_2(B)/SiO_2$	25.5	16.9	22.5	34.6	103	17.0 (14.0)
$Co–CeO_2(C)/SiO_2$	24.6	23.5	9.1	42.7	281	16.5
$Co–CeO_2(D)/SiO_2$	23.9	25.0	5.1	43.2	245	18.5
25 wt% Co/SiO_2	25.2	28.4	–	46.1	293	30.0 (30.0)

( ): Data from TEM.
[a]Calcined at 823 K.
[b]Hydrogen, nitrogen, carbon <0.3 wt%.
[c]Calculated from XRD data.

After calcination of sample Co–CeO_2(A)/SiO_2 under air at 1173 K, CeO_2 and orthorhombic cobalt silicate Co_2SiO_4 were detected by XRD. No definite structure between cobalt and cerium could be observed. This is different from catalysts with lanthanum oxide, which formed under the same conditions, a perovskite structure $LaCoO_3$.

The mean particle sizes of Co_3O_4 (derived from the broadening of the (3 1 1) line of Co_3O_4 in the diffraction pattern) are reported in Table 1 for all catalysts. These values are very close (from 16.5 to 20.5 nm), whatever the cerium content. However, we can observe that the addition of cerium leads to Co_3O_4 particles significantly smaller (by about 30%) than for the unpromoted Co/SiO_2 catalyst.

Transmission electron microscopy analyses of, for example, Co–CeO_2(B)/SiO_2 show the existence of a well defined phase, largely composed of cobalt oxide particles (Fig. 2), as confirmed by EDX. The size distribution of these particles is homogeneous, around 14.0 nm, which is slightly smaller than what was calculated from XRD. Ceria is observed as platelets (Fig. 2). Further magnification shows, at the edge of these aggregates, small particles (less than 10 nm) of CeO_2 in contact with particles of cobalt oxide.

Surface analysis by XPS of sample Co–CeO_2(A)/SiO_2 confirms the presence of CeO_2 and Co_3O_4. However, the amount of cerium on the surface is lower than in the bulk while the surface concentration of silica is much higher than expected, as also found on Co/SiO_2 [34] (Table 2).

3.2. *Reduction of Co–CeO_2/SiO_2 and Co/CeO_2 catalysts*

The determination of the amount of reduced cobalt is very important in Fischer–Tropsch synthesis since it has been shown that the presence of unreduced cobalt species can change the nature of the adsorption sites of carbon monoxide [37,38] and lead to modifications of the activity and selectivity [39–41]. We have therefore studied the influence of the cerium oxide promoter on the reducibility of cobalt.

3.2.1. *Ceria reduction*

We first studied the reducibility of ceria in the absence of cobalt. Two supports, CeO_2 (36 $m^2\,g^{-1}$) and CeO_2/SiO_2 (174 $m^2\,g^{-1}$) corresponding to the stoichiometry of the Co–CeO_2(A)/SiO_2 catalyst, were prepared using the same technique of preparation.

In TPR profiles (Fig. 3), two reduction peaks can be observed, at 823 K and beyond 1133 K. Following [42] they can be attributed to the existence of two types of oxygen anions in CeO_2: surface oxygens situated in a tetrahedral coordination site bound to one Ce^{4+} ion (reduction around 773 K) and bulk oxygens bound to Ce^{4+} reducible beyond 1023 K.

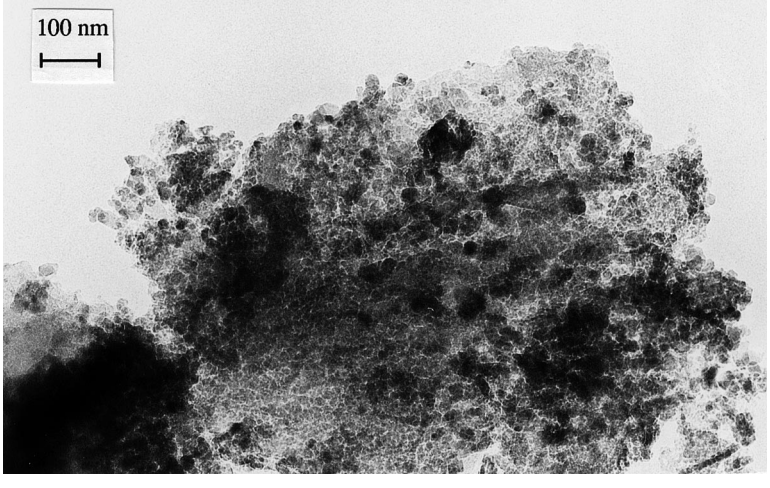

Fig. 2. Transmission electron micrograph for the Co–CeO_2(B)/SiO_2 catalyst.

Table 2
Elemental surface composition of Co/SiO_2, $Co–CeO_2$ and $Co–CeO_2(A)/SiO_2$ catalysts, compared with the theroretical bulk composition

Catalyst		Surface atomic ratio	Theoretical bulk atomic ratio
$Co–CeO_2$	Co/Ce	0.90[a]	1.15
$Co–CeO_2(A)/SiO_2$	Co/Si	1.10[b]	1.56
	Co/Ce	1.80	1.56
	Ce/Si	0.60	1.00
Co/SiO_2	Co/Si	0.12	0.40

[a]Co/Ce corresponds to the ratio of the Co2p peak area and the Ce3d peak area.
[b]Co/Si corresponds to the ratio of the Co2p peak area and the Si2p peak area.

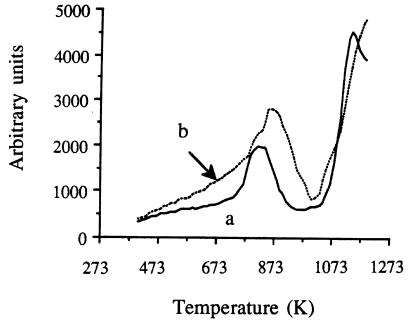

Fig. 3. TPR profiles for the CeO_2 ($36\ m^2\ g^{-1}$) (a) and CeO_2/SiO_2 ($174\ m^2\ g^{-1}$) (b) samples. (Experimental conditions: temperature increase with a $15\ K\ min^{-1}$ slope, 6% H_2/He; total flow rate: $50\ ml\ min^{-1}$; catalyst weight: 0.20 g.)

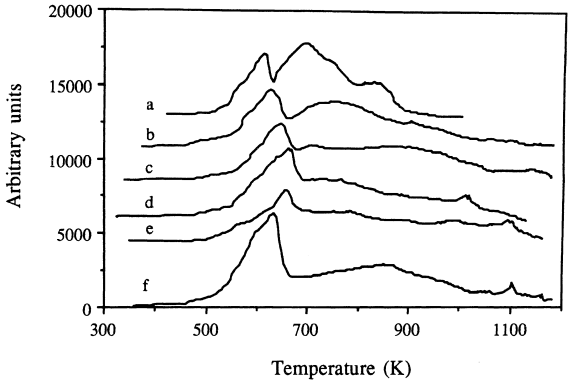

Fig. 4. TPR profiles for the $Co–CeO_2$ (a), $Co–CeO_2(A)/SiO_2$ (b), $Co–CeO_2(B)/SiO_2$ (c), $Co–CeO_2(C)/SiO_2$ (d), $Co–CeO_2(D)/SiO_2$ (e) and Co/SiO_2 (f) catalysts. (Experimental conditions: temperature increase with a $15\ K\ min^{-1}$ slope; 6% H_2/He; total flow rate: $50\ ml\ min^{-1}$; catalyst weight: 0.20 g.)

The relative intensity of these two TPR peaks is closely related to the specific area [43]. After reduction at 673 K, both samples were reoxidized by pulses of oxygen. CeO_2 supported on silica exhibited a much higher oxygen consumption than unsupported CeO_2 (8.8 μmol instead of 1.8). The corresponding stoichiometries are $CeO_{1.83}$ for the high surface area sample and $CeO_{1.97}$ for CeO_2 with reduction percentages (from Ce^{4+} to Ce^{3+}) of 34% and 6%, respectively. These results show that our CeO_2/SiO_2 sample exhibits the same reducibility properties as a high surface area industrial ceria ($115\ m^2\ g^{-1}$) for which a 25–30% reduction was found at temperatures between 673 and 723 K [44,45]. The study of the reduction of $Co–CeO_2(A)/SiO_2$ will allow to show whether similar effects can be observed when cobalt is present and whether a partial reduction of ceria can modify the reducibility of cobalt oxide.

3.2.2. *Reduction of $Co–CeO_2/SiO_2$ catalysts*

3.2.2.1. TPR study TPR profiles of $Co–CeO_2$, Co/SiO_2 and $Co–CeO_2/SiO_2$ catalysts are represented in Fig. 4. The catalysts with higher ceria loading exhibit two reduction peaks. The first peak is progessively shifted towards lower temperatures with increasing cerium content, from 653 to 603 K (for $Co–CeO_2(D)/SiO_2$ to $Co–CeO_2(A)/SiO_2$ samples). When compared with Co/SiO_2, this first peak (which is observed at 623 K with the unpromoted catalyst) can be attributed to the reduction of Co_3O_4 into metallic cobalt via CoO. It seems therefore that the reduction of Co_3O_4 is favoured when the amount of cerium is important (>40 wt%), as also shown with Ni/CeO_2 and Ni/

SiO_2 [46], but cerium in small amounts seems to hinder the cobalt reduction.

The second peak, observed at 693 K for Co–CeO_2 and at about 753 K for Co–CeO_2(A)/SiO_2 is clearly related with the presence of ceria since it disappears for cerium concentrations lower than 10%. Such a peak was already found by Bruce et al. [33] for Co–CeO_2. The easier reduction of ceria (lower temperature, higher degree of reduction) in the presence of a transition metal is well documented in: Ni [46,47], Pd [48], Rh [49–51]. It is generally interpreted in terms of a spill-over process of hydrogen from the metal (Pd [48]) to ceria. Such a possibility is most likely in our catalysts supported on silica and is reinforced by the observation of cobalt particles in close contact with ceria in our TEM micrographs.

Since both cobalt and cerium oxides can be reduced, the reduction degree of cobalt will be difficult to evaluate. In Table 3, we show the total degree of reduction of our various catalysts. They were calculated from the hydrogen consumption up to 773 K (TPR). The results show that the reduction degree increases with increasing cerium oxide content. However, Co/SiO_2 is more reduced than the catalysts which contain ceria and a little amount of the latter is enough to decrease significantly the percentage of reduction of the catalyst (45% for Co–CeO_2(D)/SiO_2 and 73% for Co/SiO_2). One possible interpretation for the easier reduction of cobalt when it is supported on silica rather than on ceria might be that ceria uses for its own reduction some of the hydrogen necessary for the reduction of cobalt. XPS, which allows to follow independently the reduction of CeO_2 and Co_3O_4, is more likely to give a clear answer to that question.

After reduction at 673 K, the main crystalline phase is fcc metallic cobalt, as detected by XRD. The particle size of Co_3O_4 after reoxidation under oxygen (1.5% O_2/He at 673 K) is given in Table 3. The values are systematically lower than after calcination (Table 1), which means that no sintering occurred during the reduction.

3.2.2.2. XPS study XPS analyses were performed on Co–CeO_2 and Co–CeO_2(A)/SiO_2 after reduction at 543, 643, 673 and 773 K. The corresponding spectra are given in Figs. 5 and 6.

The curve fitting process of XPS Ce3d spectra has been explained in detail elsewhere [52]. Let us recall briefly that each level is composed of three structures for CeO_2 (Ce^{4+}) and two more when Ce_2O_3 (Ce^{3+}) is also present. The different $Ce3d_{5/2}$ ($3d_{3/2}$) contribu-

Table 3
Reduction degree at 673 K and estimation of the mean cobalt metal crystallite size by measurement of the Co_3O_4 particle size after reoxidation for the Co–CeO_2, Co–CeO_2/SiO_2 and Co/SiO_2 catalysts

Catalyst	Reduction degree (%)[a]	Cobalt particle size (nm)[b]
Co–CeO_2	62	20.5
Co–CeO_2(A)/SiO_2	66	17.0
Co–CeO_2(B)/SiO_2	54	16.5
Co–CeO_2(C)/SiO_2	51	16.0
Co–CeO_2(D)/SiO_2	45	13.5
Co/SiO_2	73	24.0

[a]Data established by measuring the hydrogen consumption during the TPR.
[b]Calculated from (3 1 1) diffraction line broadening of Co_3O_4.

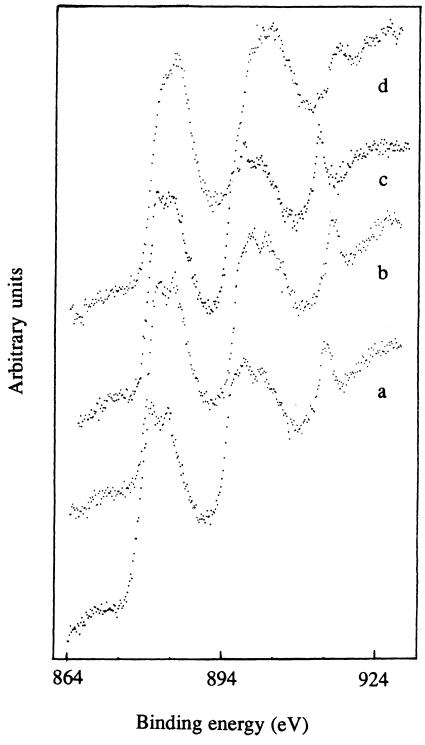

Fig. 5. Cerium 3d XP spectra of the Co–CeO_2(A)/SiO_2 catalyst reduced at 543 (a), 643 (b), 673 (c) and 773 K (d).

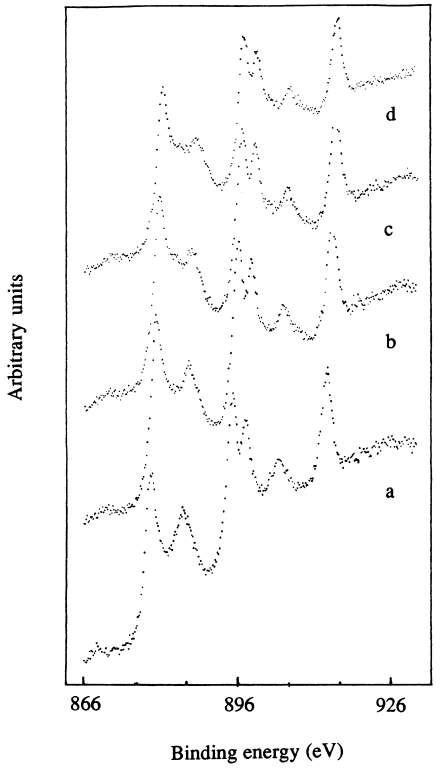

Fig. 6. Cerium 3d XP spectra of the Co–CeO_2 catalyst reduced at 543 (a), 643 (b), 673 (c) and 773 K (d).

tions are assigned following Burroughs et al. [53]: v and v'' (u and u'') are attributed to a mixing of (5d 6s)^{0}4f^2 O2p^4 and (5d 6s)^{0}4f^1 O2p^5 configurations for CeO_2, v''' (u''') to the final state (5d 6s)^{0}4f^0 O2p^6 for CeO_2 and v_0 and v' (u_0 and u') to a mixing of (5d 6s)^{0}4f^2 O2p^4 and (5d 6s)^{0}4f^1 O2p^5 configurations for Ce_2O_3.

A progressive reduction of CeO_2 will therefore result in a decrease of 4f^0 (v''' and u''') structures and an increase in v' and u' at the expense of v'' and u''; v_0 and u_0 are not easy to detect in raw spectra, due to overlapping with v and u (Figs. 5 and 6). The interpretation of the Ce3d spectrum of a partially

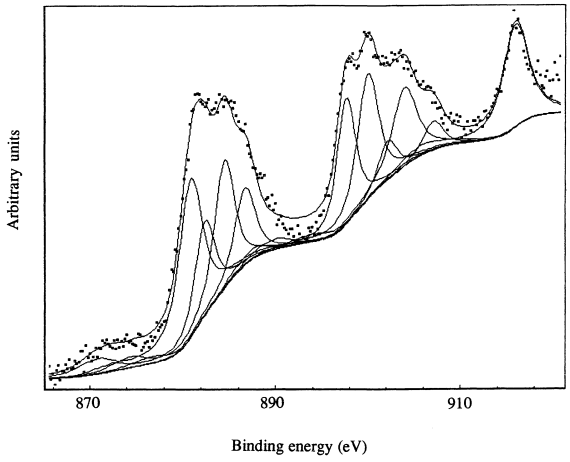

Fig. 7. Decomposed Ce3d XP spectrum for the Co–CeO_2(A)/SiO_2 catalyst reduced at 673 K.

reduced sample will imply the analysis of 10 peaks (5×2, taking into account the spin orbit coupling). In Fig. 7, we give for example the decomposition of the XPS spectrum obtained after reduction at 673 K for Co–CeO_2(A)/SiO_2. The binding energies of all 10 peaks are given in Table 4.

After decomposition, the degree of reduction can therefore be calculated following the equation [44]:

$$Ce^{III}(\%) = \frac{S_{v_0} + S_{v'} + S_{u_0} + S_{u'}}{\sum(S_v + S_u)} \times 100.$$

XPS Co2p spectra were also recorded under the same conditions. They are reported in Figs. 8 and Fig. 9 for Co–CeO_2(A)/SiO_2 and Co–CeO_2 catalysts, respectively.

The percentages of reduction of Co and Ce for the same two systems and also of Co in Co/SiO_2 [34] are given in Table 5. After decomposition of the spectra, the amount of reduction was calculated from the ratio between metallic Co and all Co contributions: Co^0 at 777.7 eV, octahedral Co^{II} (CoO) at 781.7 eV and octahedral Co^{III} (Co_3O_4) at 779.8 eV for $Co2p_{3/2}$ and the corresponding peaks for $Co2p_{1/2}$ levels.

Table 4
Binding energies of Ce3d for the Co–CeO_2(A)/SiO_2 catalyst reduced at 673 K

Peak	v_0	v	v'	v''	v'''	u_0	u	u'	u''	u'''
Binding energy (eV)	880.6	882.0	884.2	886.4	897.3	899.7	901.8	903.7	906.8	915.6

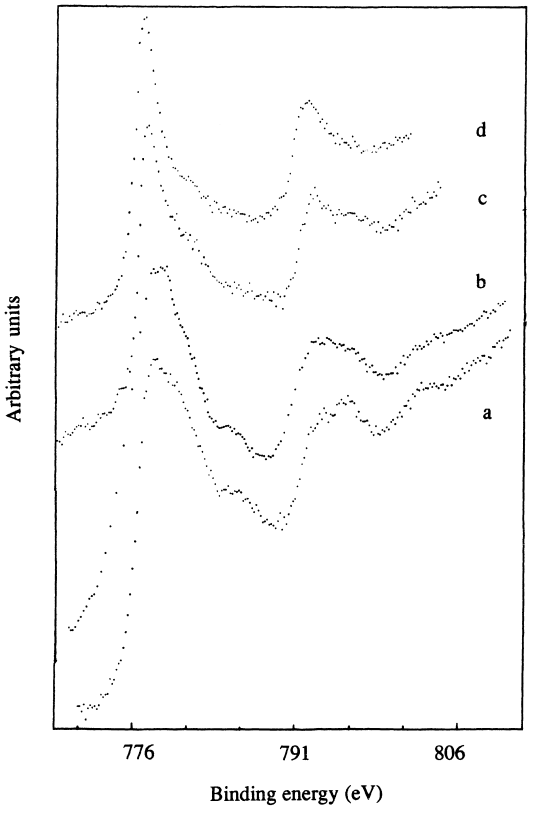

Fig. 8. Cobalt 2p XP spectra of the Co–CeO_2(A)/SiO_2 catalyst reduced at 543 (a), 643 (b), 673 (c) and 773 K (d).

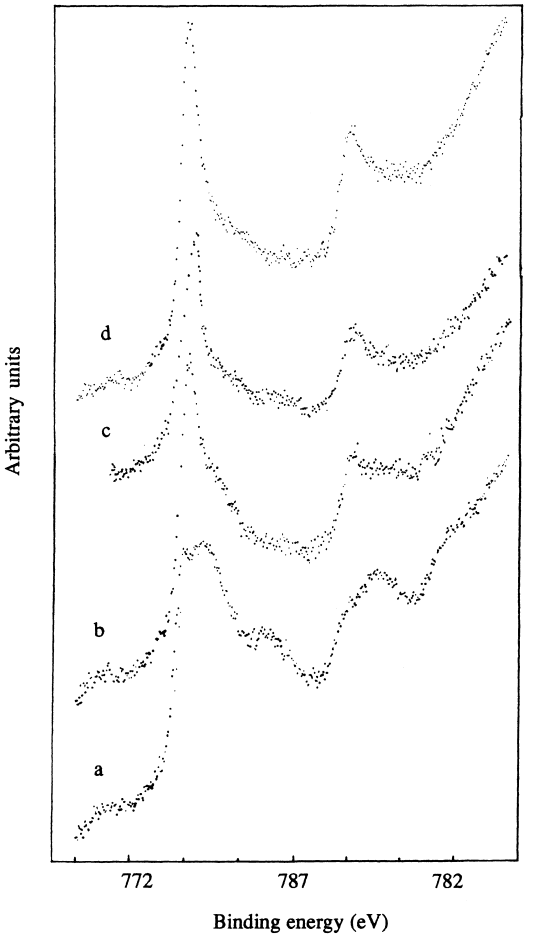

Fig. 9. Cobalt 2p XP spectra of the Co–CeO_2 catalyst reduced at 543 (a), 643 (b), 673 (c) and 773 K (d).

Table 5 shows that at 543 K the surface reduction of cobalt in Co–CeO_2(A)/SiO_2 and Co–CeO_2 is 54% and 37%, respectively, while in Co/SiO_2 the reduction does not proceed any further than CoO (48% octahedral Co^{II} and no detectable metallic contribution). This result shows that surface cobalt is more readily reduced when ceria is present. The percentage of reduction of ceria in Co–CeO_2(A)/SiO_2 is high (50%) and corresponds to $CeO_{1.75}$, significantly

Table 5
Surface reduction degree established by XPS for the Co/SiO_2, Co–CeO_2(A)/SiO_2 and Co–CeO_2 catalysts reduced at 543, 643, 673 and 773 K

Reduction temperature (K)	Reduction degree (%)				
	Co/SiO_2	Co–CeO_2(A)/SiO_2		Co–CeO_2	
	Co^0	Co^0	Ce^{III}	Co^0	Ce^{III}
543	–	54	50	37	15
643	42	73	51	73	18
673	82	81	53	87	18
773	81	89	53	84	18

higher than on CeO_2/SiO_2 alone: 34%, which corresponds to $CeO_{1.83}$. This means that cobalt seems to favour the reduction of well-dispersed ceria, certainly by a spill-over process of hydrogen from cobalt to ceria. In Co–CeO_2, the reduction of ceria is 15% only ($CeO_{1.93}$). This reveals that the presence of cobalt plays a role less important than the dispersion state of ceria (surface specific area of 65 and 137 $m^2\ g^{-1}$ for Co–CeO_2 and Co–CeO_2(A)/SiO_2, respectively) in the reduction of ceria. The percentage of reduction of ceria does not vary up to 773 K for both ceria-promoted catalysts.

These systems are very different from Ni/CeO_2: it has been shown [46] that at 423 K nickel is completely reduced while ceria is not. A percentage of reduction corresponding to $CeO_{1.85}$ is obtained at 673 K.

The percentage of reduction of cobalt increases with increasing temperature for all three systems up to 773 K, where we obtain between 81% and 89% of metallic cobalt. At 673 K, it is approximately the same for the three samples, but significantly lower for Co/SiO_2 up to 673 K.

To summarize our reduction studies by TPR and XPS, we can conclude that the reduction of ceria depends very much on its dispersion on the support, whether cobalt is present or not. Thus, the metallic cobalt help for the reduction of ceria is less important than in the case of nickel [46]. On the other hand, surface and bulk reduction of cobalt are kinetically favoured when ceria is present. It is therefore likely that at lower temperatures (543 and 643 K), a spill-over of hydrogen from ceria to cobalt does take place, since cobalt is more reduced when ceria is present and the amount of reduction of cobalt increases with increasing ceria content. However, the final reduction degree of cobalt, at 773 K, seems to depend very little on the reduction state of ceria and even on the presence of ceria so that it will be possible to compare directly the catalytic performances of these systems.

3.3. Catalytic tests

The conversion of carbon monoxide, into hydrocarbons and CO_2, together with the turn over frequency (TOF) are given in Table 6 for Co–CeO_2, Co–CeO_2/SiO_2 and Co/SiO_2. Table 7 contains the selectivities in hydrocarbons and alcohols (ROH).

Co–CeO_2/SiO_2 catalysts exhibit an activity similar to Co/SiO_2 while the conversion is very low on Co–CeO_2. There is no clear variation of the activity as a function of ceria content for Co–CeO_2/SiO_2. The activity is close to that of Co/SiO_2 and Co/TiO_2 [54] where no influence of the support was observed. Others [17,27,28,31] found a promoting effect of ceria on the catalytic activity of Co-based catalysts. However, a recent study [55] on Co–CeO_2 supported on carbon or HZT 210 zeolite showed, in accordance with our results, that the specific activities were not modified by the presence of ceria.

Concerning the selectivities, the main point is an increase in the formation of methane, when compared to Co/SiO_2. Even a small amount (5%) of ceria results in an increase in CH_4 formation (from 16% to 49%). It is also worth noting that the selectivity in C_{5+} hydrocarbons is lower than on unpromoted catalysts, although it increases with increasing ceria content. Moreover, the distribution of hydrocarbons in the C_{5+} fraction is modified. On Co–CeO_2/SiO_2 catalysts, the fraction C_5–C_{13} (gasoline) is favoured at the expense of the C_{22+} fraction (waxes). This behaviour was also

Table 6
Activity results for the Co–CeO_2, Co–CeO_2/SiO_2 and Co/SiO_2 catalysts

Catalyst	Conversion (%)			TOF (h^{-1})	Growth chain probability (α)
	CO	Hydrocarbons	CO_2		
Co–CeO_2	3.1	2.6	0.1	7.4	0.891
Co–CeO_2(A)/SiO_2	11.8	11.4	0.1	21.6	0.871
Co–CeO_2(B)/SiO_2	13.6	13.1	0.1	30.6	0.845
Co–CeO_2(C)/SiO_2	9.5	8.6	0.5	20.2	0.822
Co–CeO_2(D)/SiO_2	12.9	12.6	0.1	32.6	0.819
Co/SiO_2	10.8	10.7	0.0	25.7	0.920

Experimental conditions: T=493 K, P=2 MPa, H_2/CO=2/1, GHSV=2000 h^{-1}.

Table 7
Selectivity results for the Co–CeO_2, Co–CeO_2/SiO_2 and Co/SiO_2 catalysts

Catalyst	Selectivity (gram atom of carbon)			Hydrocarbon selectivity (wt%)					
	C_1	C_{5+}	ROH	C_1	C_2–C_4	C_5–C_9	C_{10}–C_{13}	C_{14}–C_{21}	C_{22+}
Co–CeO_2	23.0	63.9	3.1	29.2	9.5	14.9	16.8	15.4	14.2
Co–CeO_2(A)/SiO_2	27.3	60.6	2.5	34.0	9.2	12.3	15.4	15.9	13.2
Co–CeO_2(B)/SiO_2	25.1	60.0	3.1	30.1	9.7	16.6	16.6	15.7	11.3
Co–CeO_2(C)/SiO_2	39.5	47.7	3.6	46.6	8.3	10.0	13.9	14.8	6.4
Co–CeO_2(D)/SiO_2	44.2	48.1	1.2	49.1	5.6	5.8	10.4	17.5	11.6
Co/SiO_2	13.5	82.8	0.4	15.9	2.5	3.1	11.5	24.6	42.4

Experimental conditions: T=493 K, P=2 MPa, H_2/CO=2/1, GHSV=2000 h^{-1}.

observed by Barrault and Biwole [55] on a Co–CeO_2/C catalyst. We found that the selectivity towards the gasoline fraction tends to increase with increasing ceria content, together with the probability of chain growth (α), although α is lower on Co–CeO_2/SiO_2 systems than on the Co/SiO_2 catalyst (Table 6).

The modification of the hydrocarbon distribution may be attributed:

1. to the presence of smaller cobalt crystallites on Co–CeO_2/SiO_2 (13.5–17 nm) than on Co/SiO_2 (24 nm) catalysts;
2. to the unique properties of ceria which can hydrogenate CO, according to [56], leading to the selective formation of C_4 hydrocarbons (iso-alkenes)
3. to a modification of the properties of cobalt sites for hydrogen and carbon monoxide chemisorption, due to the presence of ceria.

A mechanistic approach may allow to shed some light on these questions.

3.4. Mechanistic approach

We have shown [57] that the amount of carbenic species (C_S), due to CO dissociation, which are present on the surface, is directly correlated with the catalytic activity and also with the C_{2+} selectivity obtained in Fischer–Tropsch synthesis. This means that the formation of surface carbon is the rate limiting step for the synthesis of hydrocarbons, compared to the hydrogenation of surface carbon and the polymerization of CH_x species and that surface carbon plays a part in the initiation of the chain growth process and also in the propagation process through CH_x species.

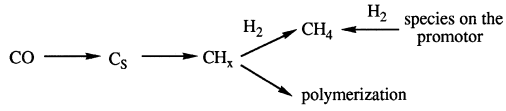

Scheme 1. Two-way methane formation: hydrogenation of CH_x species and hydrogenation of species formed on the oxide support.

Methane is formed by the hydrogenation of CH_x species, in competition with polymerization. It can also come from the hydrogenation of species present on the oxide support. This is summarized in Scheme 1.

Cerium dioxide, even in small quantity, could play a role either by modifying the dissociation of CO and therefore the concentration of CH_x species, or by favouring the hydrogenation rate of CH_x into CH_4 at the expense of the polymerization reaction. A third possibility might be the formation of methane through another process: the hydrogenation of adsorbed species (formate). More information can be derived from the adsorption of carbon monoxide and hydrogen.

Fig. 10 shows the amounts of CO adsorbed at room temperature on Co–CeO_2/SiO_2 and Co/SiO_2 catalysts. The addition of cerium results in an increase in adsorbed CO compared to the unpromoted catalyst. This effect is more important than the increase in cobalt concentration: 3.5 μmol g^{-1} for Co/SiO_2 (25 wt%) and 15.6 μmol g^{-1} for Co/SiO_2 (64 wt%) [34]. There is no correlation between the metallic particle size (Table 3) and the adsorption of CO. On the other hand, the adsorption of CO depends on the cerium content (Fig. 10). This means that, when cerium is present, there is a preferential adsorption of CO on the support. We think that this is due to the presence of hydroxyl (–OH) groups on partially

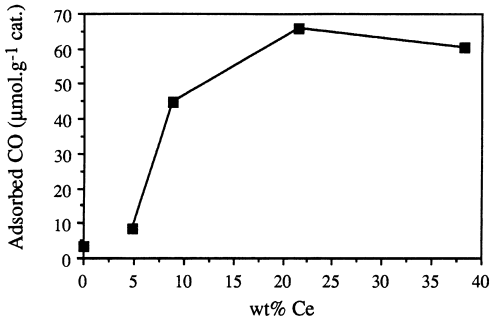

Fig. 10. Amounts of CO adsorbed on the catalytic surface versus the weight percentage of cerium for the Co/SiO_2 and $Co–CeO_2/SiO_2$ catalysts.

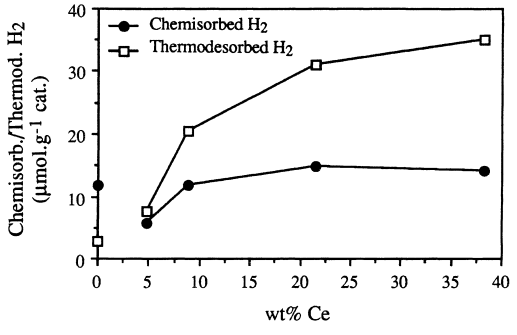

Fig. 11. Amounts of hydrogen adsorbed and desorbed on and from the catalytic surface versus the weight percentage of cerium for the Co/SiO_2 and $Co–CeO_2/SiO_2$ catalysts.

reduced ceria, as shown by XPS. Chemisorption of CO on these groups allows the formation of formate species [58,59], which are active and lead after hydrogenation to methane only.

The amounts of adsorbed and thermally desorbed hydrogen are given in Fig. 11 for $Co–CeO_2/SiO_2$ and Co/SiO_2 catalysts. Obviously, prereduced $Co–CeO_2/SiO_2$ catalysts can desorb more hydrogen than they can adsorb by chemisorption. The addition of a little quantity of cerium dioxide on Co/SiO_2 results in a decrease in the chemisorption of hydrogen ($5.6\,\mu mol\,g^{-1}$ on $Co–CeO_2(D)/SiO_2$ instead of $11.7\,\mu mol\,g^{-1}$ for Co/SiO_2). More ceria favours the adsorption of hydrogen, as shown by Guerrero-Ruiz et al. [29] on $Co–CeO_2/C$ and Barrault et al. [18] on Ni/CeO_2 catalysts. However, it is not proportional to the concentration of ceria and it reaches a limit ($14\,\mu mol\,g^{-1}$). Partially reduced ceria (CeO_{2-x}) behaves therefore as a resevoir for chemisorbed hydrogen and carbon monoxide.

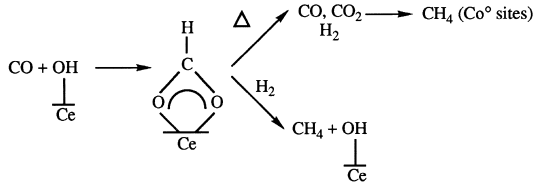

Scheme 2. Decomposition and hydrogenation of formate species formed on partially reduced ceria.

It is then most likely that a parallel formation of CH_4 via adsorbed species (formate) takes place, as shown in Scheme 2. This mechanism implies the formation of CO_2, which we actually detected in small quantities when the hydrocarbons are synthesized under high pressure while on Co/SiO_2 it is not observed. More hydrogen is desorbed with $Co–CeO_2/SiO_2$ than with Co/SiO_2 which is consistent with a higher hydrogenating power (less chain growth, more methane) when the systems are modified by CeO_2.

The study of the dissociation of carbon monoxide by means of CO disproportionation ($2CO \rightarrow C_S + CO_2$) [60] shows that, when ceria is present, more CO_2 is detected, which means that there should be more carbon on the surface. However, we will show below that the formate species, which could be formed from CO and the hydrogen remaining on the surface after reduction, can be decomposed at the temperature where the disproportionation reaction takes place (493 K). Therefore, the observed CO_2 could result both from the dissociation of surface carbon monoxide and the thermal decomposition of formate species formed on partially reduced ceria.

A study of the chemisorption of CO and H_2 followed by thermodesorption has been performed in order to get a better insight in the nature of the sites involved in the hydrogenation of CO and to try to explain the origin of the different behaviours observed in Fischer–Tropsch synthesis. This so-called temperature programmed surface reaction (TPSR) consists in preadsorbing CO at room temperature until the saturation of the surface of a catalyst prereduced at 673 K; after flushing with helium, hydrogen is introduced and the temperature programmation starts. During the analysis hydrocarbons from C_1–C_5 are produced.

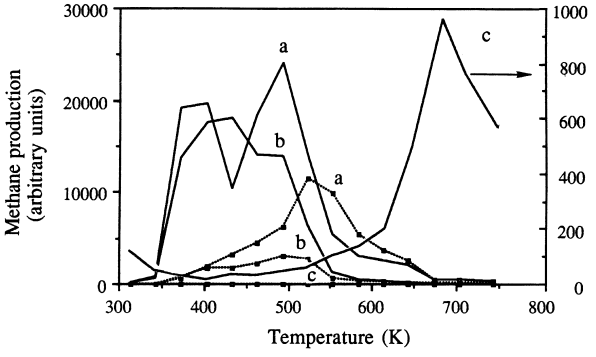

Fig. 12. Production of methane during the TPSR for the Co–CeO_2(A)/SiO_2 (a), Co/SiO_2 (b) catalysts and for the CeO_2/SiO_2 (c) support (———) and after passivation (- - -■- - -).

Fig. 12 concentrates on the formation of methane during the TPSR on Co/SiO_2 and Co–CeO_2/SiO_2 catalysts. With Co/SiO_2, a peak of methane formation at about 433 K, followed by a shoulder at 493 K is observed. This shoulder, already reported by Lee and Bartholomew [61], for a 15% Co/Al_2O_3 catalyst, is related to CO associatively chemisorbed on the catalyst. It is worth noting that the contribution of this shoulder increases with decreasing cobalt reduction [62]. With Co–CeO_2(A)/SiO_2, the reduction degree of which is the same as the unpromoted system, two peaks of methane production are observed with maxima at 373–403 and 493 K. The support treated under the same experimental conditions gives a single peak at 673 K. No C_{2+} hydrocarbon was formed on the support, which means that there is no chain growth if cobalt is not present.

In order to identify the nature of the sites (metallic or oxide phase) at 433 and 493 K, all three samples were passivated with diluted oxygen (2.5% O_2/He) at room temperature and the same adsorption process of CO and introduction of hydrogen was used. The resulting methane production is given in Fig. 12. For Co/SiO_2, the peak at 433 K is much smaller while the peak at 493 K is still strong. For Co–CeO_2(A)/SiO_2, the peak at 433 K has completely vanished. These two results show that passivation induces the suppression of the first peak which corresponds to the presence of a purely metallic site (metallic cobalt). A single peak is observed at somewhat a higher temperature (523 K) with Co–CeO_2(A)/SiO_2, reinforcing the hypothesis of the existence of some non-metallic sites. The production of methane at 493 K is due to the interaction between cobalt and ceria. This is confirmed by the fact that the area of the methane peak is smaller after exposure to oxygen and also because with the CeO_2/SiO_2 support the passivation treatment does not bring any modification of the methane production (same intensity, same temperature). We suggest that on the support, formate species are formed which are hydrogenated on metallic cobalt. Following Lee and Bartholomew [61], we can suppose that metallic particles, surrounded or covered by an oxide layer, are not accessible to reoxidation at low temperature. Some metallic particles would be left for the decomposition of formate species.

These experiments allowed us to confirm that on Co–CeO_2/SiO_2 two reactions of CO hydrogenation occur. The first reaction, which takes place on metallic cobalt proceeds through the dissociation of carbon monoxide and leads to chain growth. The second reaction would be the hydrogenation of formate species, the necessary hydrogen coming from a metallic site in close contact with the rare earth oxide and/or being stored on reduced ceria.

4. Conclusion

The addition of various amounts of cerium dioxide modifies significantly the properties of Co/SiO_2 catalysts in Fischer–Tropsch synthesis under pressure. It results in an increase in methanation and an orientation of the selectivity towards the C_5–C_{13} fraction (gasoline) at the expense of C_{22+} hydrocarbons (waxes) while the activity (TOF) remains almost the same.

During the preparation of the catalysts, after drying, a strong interaction between cobalt and cerium was observed (formation of mixed oxalates Co–Ce). The study of the reduction of calcined samples using bulk (TPR, XRD) and surface (XPS) techniques led to the conclusion that cerium dioxide is partially reduced and that the percentage of reduction depends very much on its dispersion. The reducibility of CeO_2 supported on silica, obtained by precipitation and hydrolysis-condensation, is very much the same as that of high surface area ceria. However, the reduction of cobalt is kinetically favoured at low temperature when ceria is present in high amounts (TPR).

The study of the adsorption–desorption of CO, H_2 and TPSR of $CO+H_2$ has provided an explanation for the higher production of methane observed on Co–CeO_2/SiO_2 catalysts during the Fischer–Tropsch synthesis. Active species (formates) on partially reduced ceria, which can be hydrogenated at temperatures higher than the formation of CH_4 due to the hydrogenation of surface carbon obtained by dissociation of CO on metallic sites, can explain the higher selectivity in methane observed on Co–CeO_2/SiO_2 catalysts.

Acknowledgements

The authors would like to thank Dr. P. Chaumette for his collaboration and the Institut Français du Pétrole (IFP) for financial support. Many thanks are due to E. Schleiffer for her helpful contribution in TPD and TPSR experiments.

References

[1] J.K. Minderhoud, Shell International Research, Europ. Patent Appl. no. 84200614.0, May 1984.
[2] E. Iglesia, S.L. Soled, R.A. Fiato, Exxon Res. Ing. Co., US Patent 4 794 099, December 1988.
[3] R.A. Fiato, E. Iglesia, S.L. Soled, Exxon Res. Ing. Co., Europ. Patent Appl. no. 90313466.6, April 1990.
[4] E. Iglesia, S.L. Soled, R.A. Fiato, Exxon Res. Ing. Co., US Patent 4 960 801, October 1990.
[5] H. Beuther, C.L. Kibby, T.P. Koblinski, R.B. Pannell, Gulf Research & Development, US Patent 4 613 624, September 1986.
[6] S. Eri, J.G. Goodwin, G. Marcelin, T. Riis, Den Norske Stats Oljeselskap A.S., US Patent 4 801 573, January 1989.
[7] P. Chaumette, B. Didillon, Institut Français du Pétrole, Europ. Patent Appl. no. 0764465A1, September 1997.
[8] E. Iglesia, S.L. Soled, R.A. Fiato, G.H. Via, Stud. Surf. Sci. Catal. 81 (1994) 433.
[9] P. Chaumette, C. Verdon, A. Kiennemann, S. Boujana, Am. Chem. Soc. Div. Pet. Chem. Prep. 37 (1992) 833.
[10] H.F.J. van't Blik, R. Prins, J. Catal. 97 (1985) 188.
[11] S. Vada, A. Hoff, E. Adnanes, D. Schanke, A. Holmen, Topics Catal. 2 (1995) 155.
[12] E. Iglesia, S.L. Soled, R.A. Fiato, G.H. Via, J. Catal. 143 (1993) 345.
[13] J.G. Goodwin Jr., , Am. Chem. Soc. Div. Pet. Chem. Prep. 36 (1991) 156.
[14] R. Burch, Hydrogen effects in catalysis, in: Z. Paal, P.G. Menon (Eds.), Fundamental and Practical Applications, Chapter 13, 1985, p. 348.
[15] J.S. Rieck, A.T. Bell, J. Catal. 96 (1985) 88.
[16] G.A. Martin, Stud. Surf. Sci. Catal. 11 (1982) 315.
[17] J.S. Ledford, M. Houalla, A. Proctor, D.M. Hercules, L. Petrakis, J. Phys. Chem. 93 (1989) 6770.
[18] J. Barrault, S. Probst, A. Alouche, A. Percheron-Guegan, V. Paul-Boncour, M. Primet, Stud. Surf. Sci. Catal. 61 (1991) 357.
[19] G.-N. Sauvion, J.-F. Tempere, M.-F. Guilleux, G. Djega-Mariadassou, D. Delafosse, J. Chem. Soc., Faraday Trans. I 81 (1985) 1357.
[20] H. Schaper, E.B.M. Doesburg, P.H.M. De Korte, L.L. Van Reijen, Appl. Catal. 14 (1985) 371.
[21] T. Inui, M. Funabiki, M. Suehiro, T. Sezume, J. Chem. Soc., Faraday Trans. I 75 (1979) 787.
[22] J. Barrault, C. Renard, Appl. Catal. 14 (1985) 133.
[23] R. Kieffer, A. Kiennemann, M. Rodriguez, S. Bernal, J.M. Rodriguez-Izquierdo, Appl. Catal. 42 (1988) 77.
[24] N. Takahashi, T. Mori, A. Miyamoto, T. Haltori, Y. Murakami, Appl. Catal. 38 (1998) 61.
[25] J. Barrault, A. Guilleminot, J.C. Achard, V. Paul-Boncour, A. Percheron-Guegan, Appl. Catal. 21 (1986) 307.
[26] J.S. Rieck, A.T. Bell, J. Catal. 99 (1986) 278.
[27] S. Vada, A.M. Kazi, F.K. Bedu-Addo, B. Chen, J.G. Goodwin Jr., Stud. Surf. Sci. Catal. 81 (1994) 443.
[28] J. Barrault, A. Guilleminot, J.C. Achard, V. Paul-Boncour, A. Percheron-Guegan, L. Hilaire, M. Coulon, Appl. Catal. 22 (1986) 273.
[29] A. Guerrero-Ruiz, A. Sepulveda-Escribano, I. Rodriguez-Ramos, Appl. Catal. A 120 (1994) 71.
[30] N. Barry, B.P. Internat. Limited, Europ. Patent Appl. no. 0209980, January 1987.
[31] Y. Fujitami, H. Muraki, S. Kondo, Jpn. Kokai Tokkyo Koho Jpn. US Patent 4 801 620, January 1989.
[32] L.A. Bruce, H. Hoang, A.E. Hughes, T.W. Turney, Stud. Surf. Sci. Catal. 81 (1994) 427.
[33] L.A. Bruce, H. Hoang, A.E. Hughes, T.W. Turney, Appl. Catal. A 100 (1993) 51.
[34] B. Ernst, S. Libs, P. Chaumette, A. Kiennemann, Appl. Catal. (1997), accepted for publication.
[35] B. Ernst, A. Kiennemann, P. Chaumette, Preprint of the 213th American Chemical Society National Meeting, San Francisco, 13–17 April 1997, p. 637.
[36] A. Bensalem, F. Bozon-Verduraz, M. Delamar, G. Bugli, Appl. Catal. A 121 (1995) 81.
[37] J. Rathousky, A. Zukal, A. Lapidus, A. Krylova, Appl. Catal. A 79 (1991) 167.
[38] A. Lapidus, A. Krylova, V. Kazanskii, V. Borovkov, A. Zaitsev, J. Rathousky, A. Zukal, M. Jancalkova, Appl. Catal. 73 (1991) 65.
[39] W.H. Lee, C.H. Bartholomew, J. Catal. 120 (1989) 256.
[40] W.-J. Wang, Y.-W. Chen, Appl. Catal. 77 (1991) 223.
[41] A. Lapidus, A. Krylova, J. Rathousky, A. Zukal, M. Jancalkova, Appl. Catal. A 80 (1992) 1.
[42] H.C. Yao, Y.F. Yu Yao, J. Catal. 86 (1984) 254.
[43] M.L.F. Johnson, J. Mooi, J. Catal. 103 (1987) 502.
[44] A. Laachir, V. Perrichon, A. Badri, J. Lamotte, E. Catherine, J.C. Lavalley, J. El Fallah, L. Hilaire, F. Le Normand, E.

Quéméré, G.N. Sauvion, O. Touret, J. Chem. Soc., Faraday Trans. 87 (1991) 1601.
[45] V. Perrichon, A. Laachir, G. Bergeret, R. Fréty, L. Tournayan, O. Touret, J. Chem. Soc., Faraday Trans. 90 (1994) 773.
[46] J. Barrault, A. Alouche, V. Paul-Boncour, L. Hilaire, A. Percheron-Guegan, Appl. Catal. 46 (1989) 269.
[47] E. Ramasoron, J.F. Tempere, M.F. Guilleux, F. Vergand, H. Roulet, G. Dufour, J. Chem. Soc., Faraday Trans. 88 (1992) 1211.
[48] A. Bensalem, F. Bozon-Verduraz, V. Perrichon, J. Chem. Soc., Faraday Trans. 91 (1995) 2185.
[49] A. Trovarelli, C. de Leitenburg, G. Dolcetti, J.L. Lorca, J. Catal. 151 (1991) 111.
[50] J. El Fallah, S. Boujana, H. Dexpert, A. Kiennemann, J. Majerus, O. Touret, F. Villain, F. Le Normand, J. Phys. Chem. 95 (1991) 257.
[51] J. Cunningham, D. Cullinane, J. Sanz, J.M. Rojo, X.A. Soria, J.L.G. Fierro, J. Chem. Soc., Faraday Trans. 88 (1992) 3233.
[52] M. Romeo, K. Bak, J. El Fallah, F. Le Normand, L. Hilaire, Surf. Interface Anal. 20 (1993) 508.
[53] P. Burroughs, A. Hamnett, A.F. Orchard, G. Thorton, J. Chem. Soc., Dalton Trans. (1976) 1686.
[54] E. Iglesia, S.L. Soled, R.A. Fiato, J. Catal. 137 (1992) 212.
[55] J. Barrault, N. Biwole, Bull. Soc. Chim. Belg. 104 (1995) 149.
[56] K. Maruya, A. Inaba, T. Maehashi, K. Domen, T. Onishi, J. Chem. Soc., Chem. Commun. (1985) 487.
[57] P. Chaumette, Ph. Courty, A. Kiennemann, B. Ernst, Topics Catal. 2 (1995) 117.
[58] C. Binet, A. Jadi, J.C. Lavalley, J. Chim. Phys. 89 (1992) 1779.
[59] C. Li, Y. Sakata, T. Arai, K. Domen, K. Muruya, T. Onishi, J. Chem. Soc., Faraday Trans. I 85 (1989) 1451.
[60] B. Ernst, J.P. Hindermann, A. Kiennemann, submitted for a special issue in memory of Pr. A. Andreev, Bulgarian Academy of Sciences, October 1997.
[61] W.H. Lee, C.H. Bartholomew, J. Catal. 120 (1989) 256.
[62] B. Ernst, Ph.D. Thesis, University Louis Pasteur, Strasbourg, January 1997.